Comparison of poly(ethylene oxide) crystal orientations and crystallization behaviors in nano-confined cylinders constructed by a poly (ethylene oxide)-*b*-polystyrene diblock copolymer and a blend of poly(ethylene oxide)-*b*-polystyrene and polystyrene ☆

Ping Huang [a], Ya Guo [a], Roderic P. Quirk [a], Jrjeng Ruan [a], Bernard Lotz [b], Edwin L. Thomas [c], Benjamin S. Hsiao [d], Carlos A. Avila-Orta [d], Igors Sics [d], Stephen Z.D. Cheng [a,*]

[a] *Maurice Morton Institute and Department of Polymer Science, The University of Akron, Akron, OH 44325-3909, USA*
[b] *Institut Charles Sadron, 6 Rue Boussingault, Strasbourg 67083, France*
[c] *Department of Materials Science and Engineering, Massachusetts Institute of Technology, Cambridge, MA 02139, USA*
[d] *Department of Chemistry, The State University of New York at Stony Brook, Stony Brook, NY 11794-3400, USA*

Abstract

A poly(ethylene oxide)-*b*-polystyrene (PEO-*b*-PS) diblock copolymer with a number average molecular weight of PEO blocks, $M_n^{PEO} = 8.8$ kg/mol, and a number average molecular weight of PS blocks, $M_n^{PS} = 24.5$ kg/mol, (volume fraction of the PEO blocks, f_{PEO}, was 0.26) exhibited a hexagonal cylinder (HC) phase structure. Small angle X-ray scattering results showed that the PEO cylinder diameter was 13.3 nm, and the hexagonal lattice was $a = 25.1$ nm. The cylinder diameter of this HC phase structure was virtually the same as that in the blend system constructed by a PEO-*b*-PS diblock copolymer ($M_n^{PEO} = 8.7$ kg/mol and $M_n^{PS} = 9.2$ kg/mol) and a PS homo-polymer ($M_n^{PS} = 4.6$ kg/mol) in which the f_{PEO} was 0.32. The cylinder diameter in this blend sample was 13.7 nm and the hexagonal lattice was $a = 23.1$ nm. Comparing crystal orientation and crystallization behaviors of this PEO-*b*-PS copolymer with the blend, it was found that the crystal orientation change with respect to crystallization temperature was almost identical. This is attributed to the fact that in both cases the PEO block tethering densities and confinement sizes are very similar. This indicates that when the M_n^{PS} of PS homo-polymer is lower than the PS blocks, the PS homo-polymer is located inside of the PS matrix rather than at the interface between the PEO and PS in the HC phase structure. On the other hand, a substantial difference of crystallization behaviors was observed between these two samples. The PEO-*b*-PS copolymer exhibited much more retarded crystallization kinetics than that of the blend. Based on the small angle X-ray scattering results, it was found that in the blend sample, the HC phase structure was not as regularly ordered as that in the PEO-*b*-PS copolymer, and thus, the HC phase structure contained more defects in the blend. This led to a suggestion that the primary nucleation process in the confined crystallization is a defect-controlled process. The mean crystallite sizes were estimated by the Scherer equation, and the PEO crystal sizes are on the scale of the confined size.
© 2006 Elsevier Ltd. All rights reserved.

Keywords: Confined crystallization; Copolymer; Crystal orientation

1. Introduction

In recent years, interests have been attracted to the crystallization behaviors and crystal orientations in nano-confined environments [1–23]. To generate a nano-confined

environment, one usually uses crystalline–amorphous diblock copolymers [such as poly(ethylene oxide)-*b*-polystyrene (PEO-*b*-PS) diblock copolymers] or copolymer blends (such as PEO-*b*-PS with PS or PEO homo-polymer blends). These systems are chosen because when the two components are in a strong phase separation, which is much below their order-disorder transition temperature (T_{ODT}), phase structure can be controlled to be lamellae, double gyroids, hexagonal cylinders (HC), or face-centered cubic spheres based on diblock copolymer or blend volume fractions [11]. If the glass transition temperature (T_g) of amorphous blocks (or blends) is higher than the melting temperature (T_m) of crystalline

blocks (or blends), a hard nano-confinement can be created [12].

Among those extensive studies reported about confined crystallization and crystal orientation using block copolymers as templates, the cylinder phase structure is particularly interesting to us because it constructs a two-dimensional (2D) confined environment [21–23]. It was reported that a blend of PEO-*b*-PS (with number average molecular weight of the PEO blocks $M_n^{PEO} = 8.7$ kg/mol and number average molecular weight of PS blocks, $M_n^{PS} = 9.2$ kg/mol, a copolymer that forms a lamellar phase structure) and homo-PS (with $M_n^{PS} = 4.6$ kg/mol), having a PEO volume fraction of 0.32, formed an HC phase structure [21]. Since, the M_n^{PS} of the homo-PS was lower than the M_n^{PS} of the PS blocks in the PEO-*b*-PS, the homo-PS was preferentially mixed with the PS blocks to construct this HC structure [24]. The cylinders were formed by the PEO blocks within the PS matrix, and the cylinder diameter was determined to be 13.7 nm. The T_{ODT} of this blend system was 175 °C. The glass transition of the PS (T_g^{PS}) is at 64 °C, which was higher than the melting temperature of PEO blocks ($T_m^{PEO} = 50$ °C) [21,24]. This meets the criteria of a hard confinement, $T_{ODT} \gg T_g^{PS} > T_m^{PEO}$ [12]. Using simultaneous 2D small angle X-ray scattering (SAXS) and wide angle X-ray diffraction (WAXD) techniques, it was found that the crystal orientation changes (the *c*-axes of the PEO crystals) within the cylinders were dependent on crystallization temperatures (T_c). At very low T_c (< -30 °C), PEO crystals were randomly oriented within the confined cylinders. Starting at $T_c = -30$ °C, the crystal orientation changed to be inclined with respect to the long cylinder axis, $\hat{a}$. The tilt angle between the *c*-axis of the PEO crystals and $\hat{a}$ continuously increased with increasing T_c and finally reached 90° when $T_c \geq 2$ °C [21]. Namely, the *c*-axes of the PEO crystals were now perpendicular to the $\hat{a}$ of the cylinders.

Recently, we also investigated the effect of 1D confinement of various sizes (d_{PEO}) on crystal orientation changes in the lamellar phase structure using a series of PEO-*b*-PS samples with different M_n^{PEO} and M_n^{PS} [25]. It was found that the crystal orientation, in particular, the T_c region where the *c*-axes of the PEO crystals was inclined with respect to lamellar surface normal, became narrowed with the releasing of the confined d_{PEO}.

The question becomes whether this blend system truly represents the 2D confinement for the PEO block crystal orientation changes and crystallization behaviors. We have, therefore, synthesized a PEO-*b*-PS diblock copolymer with $M_n^{PEO} = 8.8$ kg/mol and $M_n^{PS} = 24.5$ kg/mol and a PEO volume fraction of 0.26. In order to avoid the effect of the confined size on the crystal orientation changes, the M_n^{PEO} of the diblock

copolymer was selected to be 8.8 kg/mol, which is very close to the M_n^{PEO} in the blend sample. Therefore, the diblock copolymer provides the HC phase structure with an almost identical PEO cylinder diameter of 13.3 nm compared to that in the blend (13.7 nm). For the diblock copolymer, no order–disorder transition is observed by SAXS even at 190 °C; the T_{ODT} of this sample is thus higher than 190 °C. The T_g^{PS} is at 77 °C, which is higher than the melting temperature of PEO blocks ($T_m^{PEO} = 49$ °C). The criteria for hard confinement are thus met [12]. By comparing the T_c dependence of the PEO block crystal orientation changes and crystallization behaviors in this diblock copolymer with those in the blend, we expect to achieve understandings of how the 2D confined spaces and their structural regularity affect the PEO block crystal nucleation and growth.

2. Experimental section

2.1. Materials and sample preparation

The PEO-*b*-PS diblock copolymer was sequentially synthesized using anionic block copolymerization of styrene and ethylene oxide monomers. The synthetic procedures can be found elsewhere [26,27]. The PS precursor was characterized by size exclusion chromatography (SEC) using a polystyrene standard and had a M_n^{PS} of 24.5 kg/mol and a polydispersity of 1.02. The M_n^{PEO} was determined by proton nuclear magnetic resonance to be 8.8 kg/mol. Note that this M_n^{PEO} in the copolymer is very similar to that of the blend previously reported ($M_n^{PEO} = 8.7$ kg/mol) [21]. A polydispersity of 1.04 in the final diblock copolymer was determined by SEC using the universal calibration. The volume fraction of PEO blocks was 0.26. The detailed molecular characterizations are listed in Table 1. This table also includes various transition temperatures of the blend and the copolymer samples. The volume fraction of the PEO blocks (f_{PEO}) in the melt at 60 °C (listed in Table 1) was calculated based on the densities of amorphous PEO and PS, which are 1.092 and 1.035 g/cm³, respectively [26].

In order to ensure the consistency of the phase behavior, uniform sample preparation and identical thermal history were necessary. The sample was cast from a 5% (w/v) toluene solution, and the solvent was evaporated slowly under a dry nitrogen atmosphere at 50 °C to prevent crystallization of the PEO blocks. Residual solvent was removed under vacuum at 50 °C for 1 day and the sample was then annealed at 95 °C for 12 h to allow the development of micro-phase separation. In order to study crystal orientations in the block copolymer samples, the micro-phase-separated samples were subjected to

Table 1
Molecular characteristics and thermal properties of the blend and the copolymer

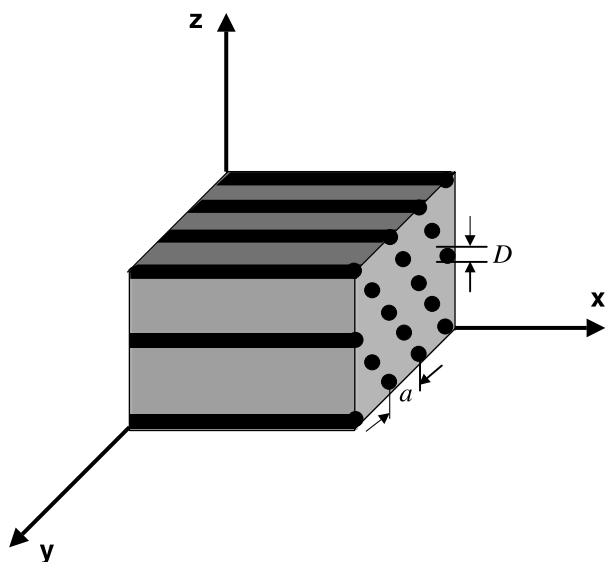| Sample	M_n (PS block) (g/mol)	M_n (PEO block) (g/mol)	M_n (PS homo) (g/mol)	f_{PEO}	T_{ODT} (°C)	T_g^{PS} (°C)	T_m^{PEO} (°C)	T_c^{PEO} (°C)
Blend	9200	8700	4600	0.32	175	~64	50	17
Copolymer	24,500	8800	–	0.26	>190	~77	49	−27

Fig. 1. Schematic drawing of the mechanically sheared sample of PEO-*b*-PS diblock copolymer with the cylindrical morphology. Two parameters of D and a are the cylinder diameter (D) and distance between the center of two neighboring cylinders (a).

a large-amplitude oscillating shear under a dry argon atmosphere at 140 °C to achieve uniform alignment of the cylindrical phase structure. The shearing geometry is shown in Fig. 1 in which the shear direction is along the *x*-axis, and the *xy* plane is the shear plane with the shear gradient direction along the *z*-axis. The apparatus set-up in our laboratory included a fixed bottom base with a hot stage and a top metal plate with tunable horizontal mobility, magnitude, and speed controlled by a motor. The shear frequency was 1 Hz, and the shear amplitude was 150%. The shear-aligned sample was further annealed at 95 °C for another 12 h in vacuum to release any residual stresses.

2.2. Equipment and experiments

Simultaneous 2D SAXS and WAXD experiments were conducted on the synchrotron X-ray beam-line X27C at the National Synchrotron Light Source in Brookhaven National Laboratory. The wavelength of the X-ray beam (λ) was 0.1366 nm. The zero pixel of the 2 D SAXS pattern was calibrated using silver behenate, with the first-order scattering vector q^* ($q^* = 4 \pi \sin\theta/\lambda$, where 2θ is the scattering angle) being 1.076 nm^{-1}. 2D WAXD were calibrated using α-AlB$_2$OB$_3$ with known crystal diffractions and air scattering being subtracted. Azimuthal profiles for 2D WAXD patterns were obtained via scans that were started on the vertical direction of the patterns. The standard deviation in determining the angular maximum was $\pm 3°$.

In order to analyze the correlation lengths (the apparent crystallite sizes) of the PEO crystals in the 2D confinement, the Scherrer equation was used:

$$D_{hkl} = \frac{K\lambda}{\beta_{hkl} \cos \theta} \tag{1}$$

where D_{hkl} was the mean crystallite size along the [hkl] direction, K was the shape factor (the Scherrer constant, a value of 0.94 was used in this study [28]), β_{hkl} was the line breadth, and θ was the half-scattering angle. Usually, β_{hkl} was taken as the half-width at half maximum (HWHM) of the (hkl) diffraction. Assuming that the diffraction peak shape obeyed a Gaussian function, Warren's correction can be used to correct instrument broadening [28]:

$$\frac{\beta_{hkl}}{B_{hkl}} = \sqrt{1 - \frac{b^2}{B_2^{hkl}}} \tag{2}$$

where B_{hkl} was the experimentally observed HWHM of the diffraction peak, and b, the HWHM of a standard specimen diffraction. To ensure a good calibration, the mean crystallite size of the standard specimen should be > 60 nm. A quartz line at 60.0° was taken for obtaining the standard, b.

DSC experiments were carried out on a Perkin–Elmer Pyris Diamond DSC to study melting behaviors of the diblock copolymer samples. The DSC was calibrated with naphthalene, benzoic acid and indium standards. The fully crystallized samples were heated at a rate of 10 °C/min. The endothermic peak temperature was taken as the T_m. The weight percentage crystallinity (w_c) was calculated using an equilibrium heat of fusion for PEO crystals (8.66 kJ/mol) [29].

Transmission electron microscopy (TEM) experiments were carried out on a Philips Tecnai 12 at an accelerating voltage of 120 kV. Thin sample sections were obtained using a Reichert Ultracut S (Leica) microtome to cut the sheared samples at -40 °C. The samples were stained under a RuO$_4$ vapor at room temperature for 30 min [30].

Isothermal crystallization experiments of PEO blocks were conducted using an Instec LN2-P2 hot stage equipped with a liquid nitrogen cooling system. The isothermal T_c was controlled to within ± 0.2 °C. The shear-aligned samples were preheated to 70 °C for 3 min and then quickly quenched to the hot stage at a preset T_c for crystallization. The lower limit of the controllable isothermal T_c was -45 °C.

3. Results and discussion

3.1. Comparing phase structures in the copolymer and the blend

Although the PEO volume fractions of these two systems are different (0.32 versus 0.26), both the diblock copolymer and the blend exhibit HC phase structures with a 2D hexagonal lateral packing. Two bright-field TEM micrographs of thin sections of the copolymer samples after RuO$_4$ staining are shown in Fig. 2(a) and (b). Since, PEO blocks are easier to be stained by RuO$_4$ than PS blocks, the PEO cylinders appear darker than the PS matrix. Fig. 2(a) roughly represents a head-on view (along the *x* direction), and Fig. 2(b) is a side view of the HC structure.

Fig. 3 shows a set of 2D SAXS patterns of the shear oriented copolymer sample after it was quenched to room temperature when the X-ray beam is along the *x* (Fig. 3(a)), *y* (Fig. 3(b)) and
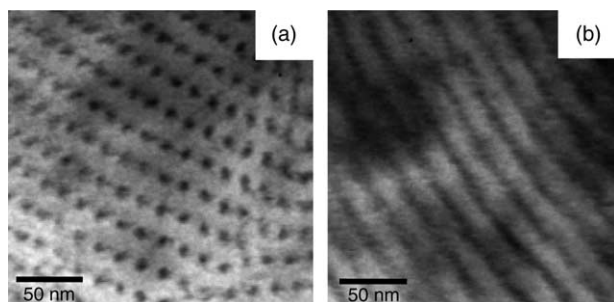
Fig. 2. Bright-field TEM micrograph of the cylinder phase morphology of the copolymer stained by RuO_4.

z (Fig. 3(c)) directions. It is evident that in the 2D SAXS pattern in Fig. 3(a), up to seven orders of reflections can be observed. They are the $(10\bar{1}0)$, $(1\bar{2}10)$, $(20\bar{2}0)$, $(21\bar{3}0)$, $(30\bar{3}0)$, $(2\bar{4}20)$ and $(31\bar{2}0)$ reflections of the HC phase structure. The relationship of these reflections is $q/q^* = 1 : \sqrt{3} : \sqrt{4} : \sqrt{7} : \sqrt{9} : \sqrt{12} : \sqrt{13}$. The six fold symmetry in this pattern clearly indicates that the cylinders in the copolymer are packed into a hexagonal lattice. In Fig. 3(a), it is also observed that a pair of the $[10\bar{1}0]$ directions is perpendicular to the shear (the xy) plane. Therefore, the $(10\bar{1}0)$ planes of the HC phase structure are oriented parallel to the xy plane. Fig. 3(b) and (c) are side views with the X-ray beam aligned to the apex (the y direction) and the side (the z direction) of the HC structure, respectively. When the HC lattice is perfectly oriented with the $(10\bar{1}0)$ planes parallel to the xy plane, only the $(10\bar{1}0)$, $(20\bar{2}0)$, and $(30\bar{3}0)$ reflections can be observed as shown in Fig. 3(b), while only the $(1\bar{2}10)$ reflection can be observed from the side as shown in Fig. 3(c). This reveals that the HC phase structure is a 'single-crystal-like' monodomain in squares with an area of at least sub-millimeters (the size of the beam).

This is distinctly different from the HC phase structure observed in the blend sample (Fig. 3 in Ref. [21]). For the SAXS patterns of the blend, only five orders of reflections could be observed when the X-ray was aligned to the x direction. The diffraction shapes were arcs rather than spots as observed in the copolymer here. In addition, the 2D SAXS patterns obtained along both the y and z directions for the blend are less different from that of the copolymer sample, indicating that the blend sample obtained from the mechanical shear is an aggregation of a few domains in the HC phase structure separated by grains and that the orientation in the xy plane is distorted.
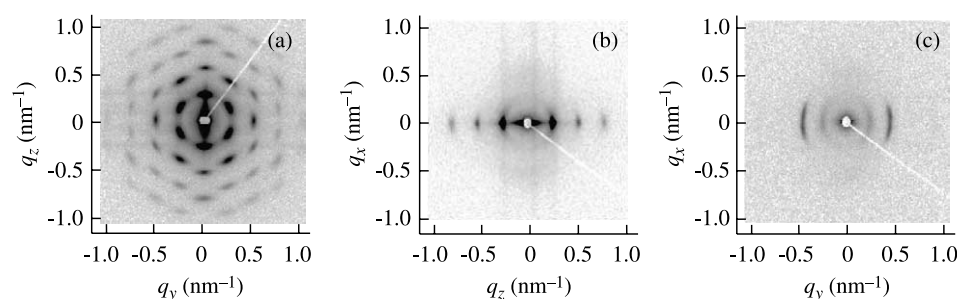
Since, the volume fractions of PEO blocks are different in these two systems, we expect that the size of these two HC phase structures (a in Fig. 1) should be different. Based on the SAXS results, $a = 25.1$ nm for the copolymer, compared with $a = 23.1$ nm for the blend [21]. On the other hand, the PEO cylinder diameter (d) values for both the samples are similar: $d = 13.3$ nm for the copolymer and 13.7 nm for the blend [21]. This is because the M_n^{PEO} values in both cases are almost identical. Furthermore, the tethering density of PEO blocks at the interface [31] is also almost identical, $0.25/nm^2$ for the copolymer and $0.26/nm^2$ for the blend sample.

3.2. Crystal orientation changes in the 2D confined cylinders

When the copolymer sample was quenched into liquid nitrogen or isothermally crystallized at different T_c values, the 2D SAXS patterns are identical to those in Fig. 3(a)–(c), indicating that the cylindrical phase morphology is retained after the sample is isothermally crystallized and the PEO blocks are crystallized within the cylinders. Fig. 4 shows 2D WAXD patterns conducted on the PEO-b-PS sample after being quickly quenched into liquid nitrogen [the crystallization temperature of PEO is estimated between -67 °C (T_g of PEO) and -50 °C], and all three 2D WAXD patterns in Fig. 4(a)–(c) show ring reflections. The inner ring is attributed to the (120) reflection (with a d-spacing of 0.463 nm) and the outer ring is the overlapped $(\bar{1}32)$, (032), (112), $(\bar{2}12)$, $(\bar{1}24)$, $(\bar{2}04)$, and (004) reflections (with d-spacing of 0.38–0.40 nm). Therefore, the PEO crystals are randomly oriented (isotropic) within the cylinders. A real space model is schematically illustrated in Fig. 4(d). It is deduced that the homogeneous primary nucleation density is very high and little crystal growth is carried out to complete the crystallization in such high undercooling. In other words, the PEO crystals are too small to 'feel' the 2D cylindrical confinement provided by the glassy PS matrix. The PEO crystal size should be smaller than 13.3 nm.

The WAXD patterns along the x and y directions for the sample isothermally crystallized at T_c values between -40 and -10 °C are shown in Fig. 5. Since, the 2D WAXD patterns obtained along both the y and z directions are identical, only the 2D WAXD pattern obtained when the X-ray was aligned to the y direction is shown here. The WAXD patterns, which were taken along the x direction (Fig. 5(a), (c), (e) and (g)) exhibit isotropic reflections with two major rings as described in

Fig. 3. Sets of 2D SAXS patterns of the copolymer at room temperature when the X-ray beam was aligned to (a) the x, (b) the y and (c) the z directions.
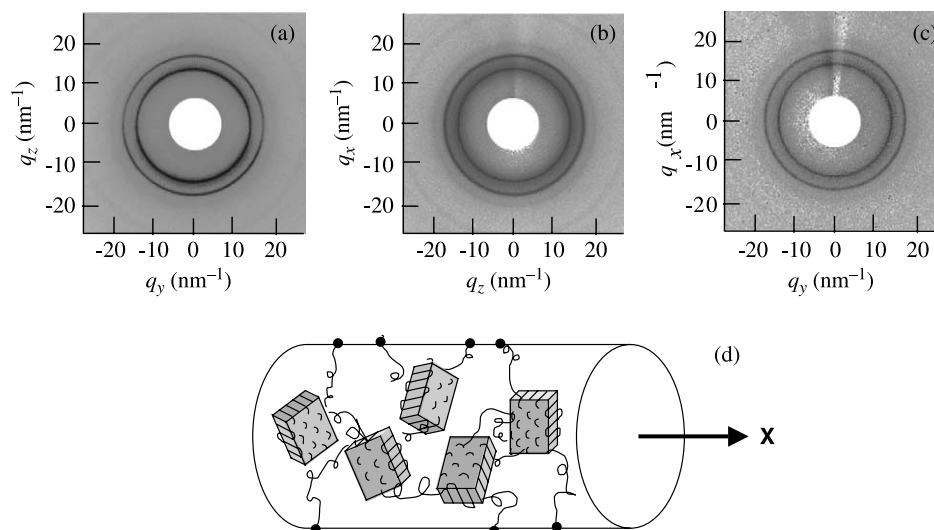
Fig. 4. Set of 2D WAXD patterns of the copolymer crystallized after being quenched into liquid nitrogen. The X-ray beam was along (a) the x, (b) the y and (c) the z directions. (d) Schematic of random crystal orientation within the confined cylinder.
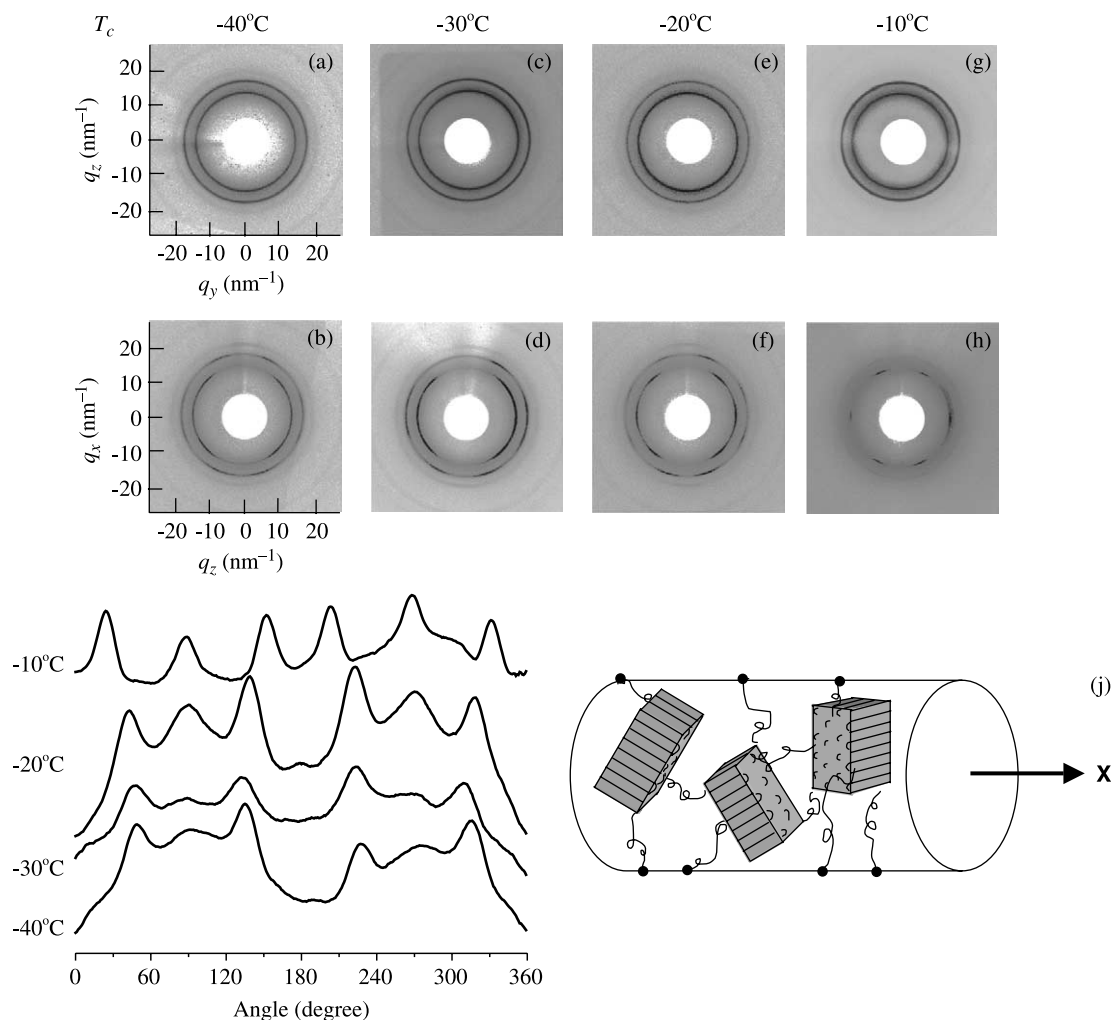

Fig. 5. Set of 2D WAXD patterns of the copolymer crystallized in the T_c region with tilted orientation of the PEO crystals. (a) $T_c = -40$ °C, the X-ray beam was along the x direction; (b) $T_c = -40$ °C, the X-ray beam was along the y direction; (c) $T_c = -30$ °C, the X-ray beam was along the x direction; (d) $T_c = -30$ °C, the X-ray beam was along the y direction; (e) $T_c = -20$ °C, the X-ray beam was along the x direction; (f) $T_c = -20$ °C, the X-ray beam was along the y direction; (g) $T_c = -10$ °C, the X-ray beam was along the x direction; (h) $T_c = -10$ °C, the X-ray beam was along the y direction, respectively; (i) azimuthal profiles of the (120) reflections on the first ring between -40 °C $\leq T_c \leq -10$ °C; (j) schematic of an inclined crystal orientation within the confined cylinder.

Fig. 4(a). This indicates that the *c*-axes of the PEO crystals are isotropic with respect to *â*; however, in the 2D WAXD patterns at different T_c values along the *y* direction as shown in Fig. 5(b), (d), (f) and (h), two pairs of the (120) reflections are located in the quadrants and another pair is on the equator. The azimuthal scanning profiles for these experimental (120) reflections at different T_c values are shown in Fig. 5(i). This reveals that the *c*-axis of the PEO crystals is tilted with respect to *â*. We define the tilting angle as the angle between the *c*-axis of the PEO crystals and *â*. It is found that with increasing T_c, these two pairs of the (120) reflections on the quadrants gradually move towards the meridian, indicating an increase of the tilting angle. A real space model is schematically illustrated in Fig. 5(j). The tilting angles are 44°, 47°, 48° and 64° for $T_c = -40, -30, -20$ and -10 °C, respectively.

When $T_c \geqq 0$ °C, the two pairs of the (120) reflections originally observed in the quadrants finally reach the meridian in the 2D WAXD pattern when the X-ray beam is aligned to the *y* direction. The WAXD pattern taken along the *x* direction still exhibits isotropic ring reflections, indicating that the PEO crystals are isotropic with respect to *â* (since they are identical to Fig. 4(a) and they are not shown again in the figure). Above $T_c = 0$ °C the 2D WAXD patterns no longer change with T_c. Fig. 6(a) and (b) show two WAXD patterns for the copolymer crystallized at $T_c = 0$ and 10 °C, respectively, when the X-ray is aligned to the *y* direction. In both the patterns, two pairs of the (120) reflections are perpendicular to each other, and they are located on both the equator and the meridian. However, the crystallinity of PEO blocks is very low when the sample is crystallized at these two T_c values (see below). This causes the low reflection intensities in Fig. 6(a) and (b). The azimuthal scanning profiles for these experimental (120) reflections at

different T_c values are shown in Fig. 6(c), indicating that the *c*-axis of PEO crystals is oriented perpendicular to *â*. These patterns can be explained using a [120]-uniaxial pattern [32]. A real space model is schematically illustrated in Fig. 6(d).

On the basis of self-seeding experiments in one of our previous studies [33], it was concluded that the crystal orientation is not determined by the primary nucleation but dominated by the initial step of crystal growth. This is because that the primary nuclei of the PEO blocks are too small to 'feel' the confined PS environment, and their orientation can be changed within the cylinders. As the PEO crystal growing, the increase of of PEO crystal sizes reaches a level that is comparable with the confined size (the cylinder diameter here), the crystal growth will be hampered. Since, the crystallization of PEO blocks is a kinetic process; the PEO crystals need to adopt an orientation that provides the most effective growth to achieve the maximum crystallinity for each crystal as long as the crystal growth kinetics permits (the growth is slow enough). The perpendicular orientation is thus only observed when the T_c is higher than 0 °C. We believe that the titled orientation of the PEO crystals is resulted from the competition between the nucleation and growth rates (see below).

A relationship between the tilting angle and T_c is plotted in Fig. 7. With increasing T_c, the tilting angle increases monotonously. When compared with the tilting angle changes with T_c for the blend previously reported [21], which are also included in Fig. 7, the results match closely in both of the cases. Therefore, the conclusion is that disregarding the system, either in the diblock copolymer or the blend, the crystal orientation changes with T_c are insensitive to the degree of perfection of the HC phase structures obtained via mechanical shearing.
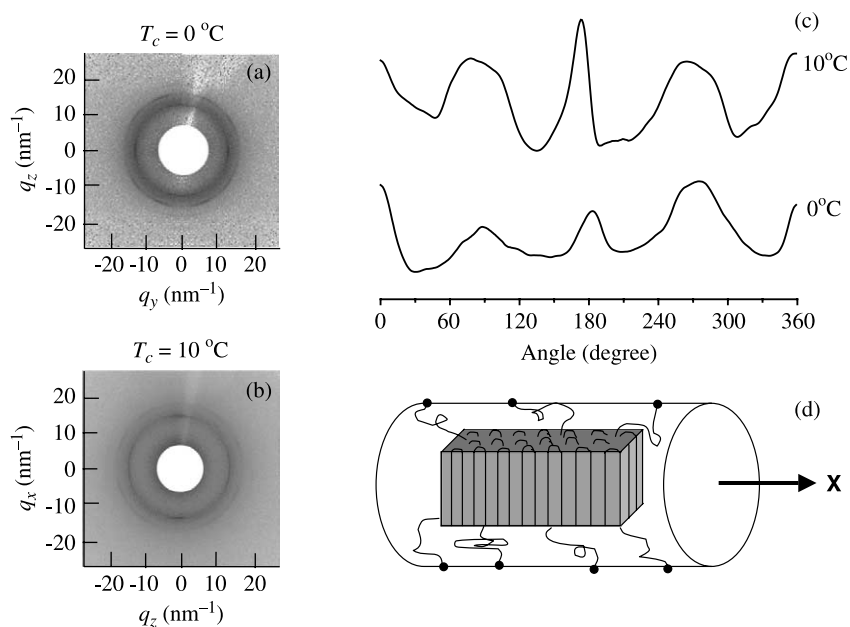

Fig. 6. Set of 2D WAXD patterns of the copolymer crystallized in the T_c region with homogeneous orientation of the PEO crystals. (a) $T_c = 0$ °C; (b) $T_c = 10$ °C, the X-ray beam was along the *y* direction; (c) azimuthal profiles of the (120) reflections on the first ring when $T_c = 0$ and 10 °C; (d) schematic of a homogeneous crystal orientation within the confined cylinder.
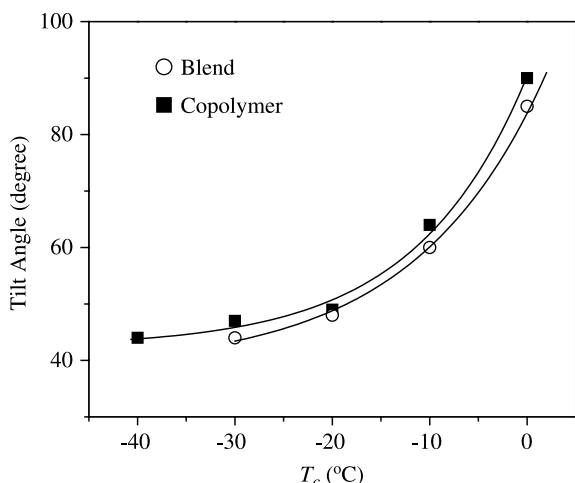
Fig. 7. Relationships between the inclined angles with respect to T_cs for the blend and the copolymer samples.

Fig. 9. Changes of the crystallinity and melting temperatures with respect to T_c for the copolymer.

3.3. Crystallization behaviors of the PEO blocks in 2D confinement

Fig. 8 shows DSC cooling and heating thermal diagrams at a rate of 10 °C/min for the copolymer sample. The exothermic peak, which represent the crystallization process of PEO blocks, is at −27 °C. This T_c value is very different from that for the blend sample, which was found to be 17 °C (Table 1, and also, see Fig. 9 in Ref. [24]). The primary nucleation in the copolymer sample is thus more difficult to form compared to that in the blend. The nucleation and crystallization behaviors of crystalline–amorphous block copolymers or blends within confined spaces having cylinders or spheres have been extensively reported [19,20,24,34–41]. In particular, a fractionated crystallization of PEO blocks in a polyethylene-b-poly(ethylene-alt-propylene)-b-poly(ethylene oxide) triblock copolymer was observed [34]. Before the sample purification, a major part of the PEO blocks were crystallized at 20 °C, and a minor part of the PEO blocks were crystallized at −20 °C. It was concluded that the crystallization at 20 °C resulted from
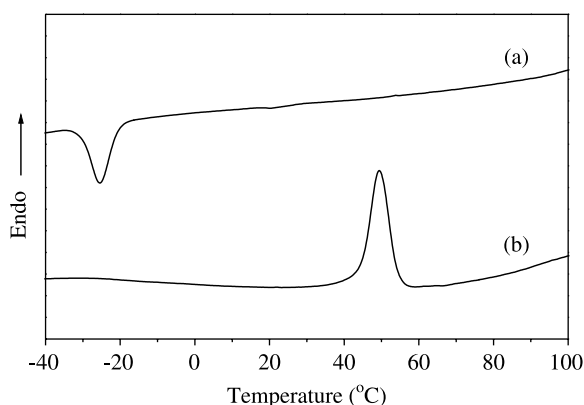

Fig. 8. DSC (a) cooling and (b) heating curves for the copolymer. The cooling and heating rate are 10 °C/min.
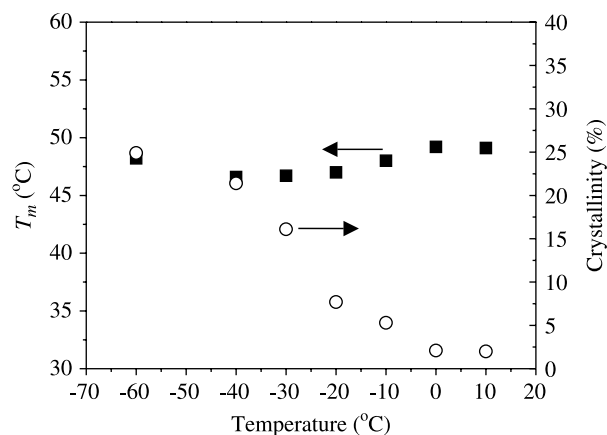
the presence of heterogeneities, since after purification, the PEO can only crystallize at −27 °C [34]. We speculate that, in the unfractionated sample, the chemical and/or architectural heterogeneities might form two types of phase structures with different abilities in confining the PEO block nucleation and crystallization.

In our two samples, only the HC phase structures exist with almost identical cylinder diameters; therefore, the very different crystallization behavior observed has to be associated with the difference of the defect density between the blend and copolymer samples. It is inevitable that the sheared samples contained a number of defects, which may connect neighboring cylinders. This would locally double or multiple the diameter size of the cylinders at the defect points and release the confinement. Aggregations of these kinds of defects may form sub-grains and grains in the structure. If the defect density is relatively high, a 3D network of the defects may also be constructed, which keeps the cylinder orientation. Since, the HC phase structure in the copolymer sample is the 'single-crystal-like' monodomain in squares the size of at least sub-millimeters compared with the domain aggregation in the blend sample, the local defects which inter-connects neighboring cylinders are much less possible in the copolymer samples. It is known that the exothermic crystallization process at 17 °C in the blend is in the heterogeneous nucleation region; while, the crystallization at −27 °C in the copolymer is in the homogeneous nucleation region. One can deduce that, in the blend, the heterogeneous nucleation is still effective due to the existence of the defects and that this should be responsible for the faster crystallization kinetics of the blend sample compared with that of the copolymer. In the copolymer, on the other hand, only the homogeneous nucleation existing within PEO cylinders can induce the crystallization. The crystallization kinetics must, therefore, be a defect-controlled process. On the other hand, a less possible reason is that the copolymer sample possesses a higher T_g (77 °C) compared with that of the blend (64 °C). In our previous work, it was found that the PEO block crystallization kinetics in the hard confinement is much more retarded than that in the soft confinement [24]. However,

the 30 °C difference of the exothermic processes observed in DSC cooling diagram should not be fully resulted from this T_g difference since the hard confinement criteria were reached for both the blend and copolymer samples.

Fig. 9 shows the T_m^{PEO} and crystallinity changes with respect to T_c for the copolymer. The T_m^{PEO} is found roughly in a range between 46 and 50 °C. The crystallinity is, however, dramatically decreased from ∼25% at −40 °C to ∼2% at 10 °C. This crystallinity is much lower than that of the blend sample at the same T_c (∼50%). This is again a suggestion that the primary nucleation process is much more difficult in the copolymer sample compared to that in the blend. In particular, when entering the heterogeneous primary nucleation region at $T_c > \sim -5$ °C, only the PEO blocks within a few PEO cylinders possess the heterogeneous nuclei that can initiate the crystallization. This leads to a very low crystallinity in the copolymer sample. As a result, the defects at which the inter-cylinder connections take place play an important role to determine the crystallization kinetics. This difference of crystallization behaviors between the copolymer and blend samples does not seem to affect the crystal orientation changes (see Fig. 7). This indicates that the defects can effectively influence the process, which relies on the material's connectivity (continuous crystallization after the nucleation) via the defect network, but they do not affect the local crystal orientation of which the vast majority of the

PEO crystals are still within in the confined cylinders in the blend sample.

3.4. Apparent crystallite size estimation using the Scherrer equation

In order to study the crystal growth dimension within the confined cylinders, we perform data analysis of the WAXD patterns along the y direction by using the Scherrer equation. Fig. 10(a) and (b) show the calculated (120) lateral crystallite sizes at different T_c for the copolymer and the blend, respectively. There are two sets of lateral crystallite sizes for both of the two samples. One is relatively short ($D_{120,s}$), which describes the mean crystallite size along the direction that is perpendicular to $\hat{a}$, and another is relatively long ($D_{120,l}$), which describes the mean crystallite size along the direction that is tilted (within the temperature region where PEO crystals have a tilted orientation with respect to $\hat{a}$) or parallel to $\hat{a}$ (within the temperature region where PEO crystals have a perpendicular orientation with respect to $\hat{a}$).

As shown in Fig. 10(a), for the copolymer within the T_c region where PEO crystals have the tilted orientations (left side of the vertical dashed line in the figure), the $D_{120,s}$ at $T_c = -40$ °C is 9.1 nm. $D_{120,s}$ slightly increases to 11.7 nm at $T_c = -10$ °C because of a decrease in the primary nucleation density of the crystals with increasing T_c. Then, the $D_{120,s}$ keeps a
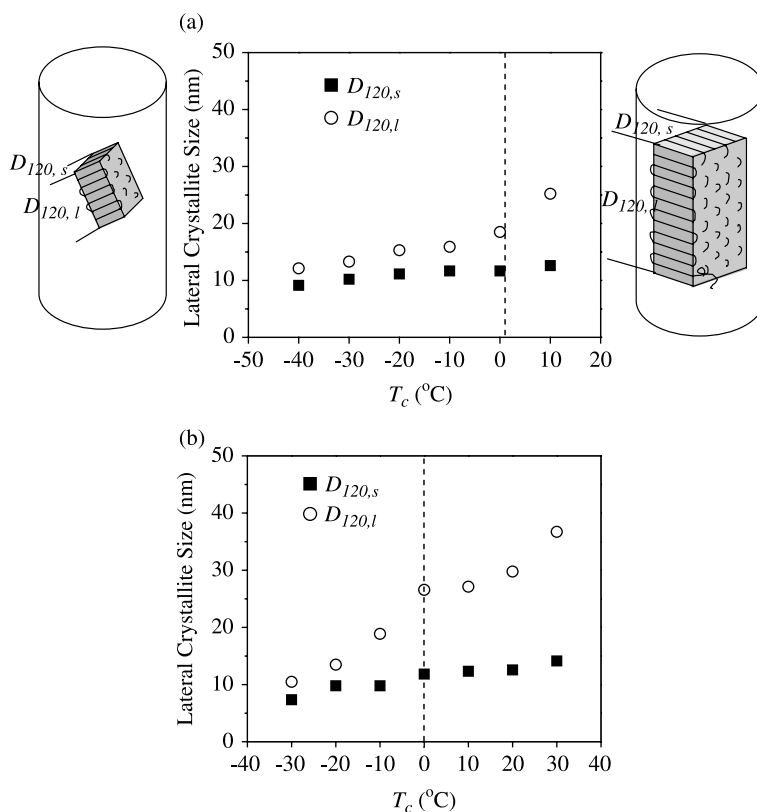

Fig. 10. Correlation length (apparent crystallite size) analyses for the (120) diffractions at different T_c values in the 2D WAXD patterns when X-ray beam is along the y direction: (a) the copolymer and (b) the blend.

constant value due possibly to the limiting PEO cylinder diameter size of 13.3 nm; therefore, this $D_{120,s}$ may reflect a true crystal size. On the other hand, the $D_{120,l}$ starts at $T_c = -40\ ^\circ$C with a length of 12.1 nm. It continuously increases to 18.5 nm at $T_c = 0\ ^\circ$C. The $D_{120,l}$ is always larger than the corresponding $D_{120,s}$, since the confinement along the $D_{120,l}$ direction is gradually released with increasing tilting angle and the primary nucleation density decreases with increasing T_c. There is a sudden increase in $D_{120,l}$ when T_c is above $0\ ^\circ$C. The $D_{120,l}$ may no longer represent the true crystal size. The nucleation density above $T_c \gtreqqless 0\ ^\circ$C is substantially decreased because of a change from homogeneous to heterogeneous nucleation. Since, in this T_c region the PEO c-axes of crystal are perpendicular to $\hat{a}$, the PEO crystals grow along the $D_{120,l}$ direction. The crystal size along this direction can only be limited by impingement of neighboring crystals within one cylinder. However, the nucleation density in this T_c region is very low, only a few cylinders possess the nuclei, and thus can be crystallized. This leads to a very low crystallinity and small possibility for the impingement to take place along the $D_{120,l}$ direction. The crystal sizes along this direction thus only depend on the crystallization time.

Fig. 10(b) shows the $D_{120,s}$ and $D_{120,l}$ crystallite size changes of the PEO crystals with respect to T_c for the blend sample. Compared with Fig. 10(a), both results are similar, roughly speaking, but not exactly identical. In the entire T_c region, the $D_{120,s}$ of the blend behaves the same as that in the case of the copolymer, which is bound by the PEO cylinder diameter of 13.7 nm. For the $D_{120,l}$ below $T_c = 0\ ^\circ$C, it starts at 10.5 nm at $T_c = -30\ ^\circ$C and increases at a faster rate with T_c compared with the copolymer sample. For example, at $T_c = 0\ ^\circ$C the $D_{120,l}$ reaches 26.6 nm. Above $T_c = 0\ ^\circ$C, the PEO crystal growth along the $D_{120,l}$ direction is again only limited by impingement of neighboring crystals. Therefore, the $D_{120,l}$ is much larger than $D_{120,s}$ in this temperature region. Also, the $D_{120,l}$ may reach a limit above which it does not represent the true crystal size along this direction. A sudden change of the $D_{120,l}$ at $T_c = 0\ ^\circ$C is not as evident as that in the copolymer. The difference on the $D_{120,l}$ between the copolymer and the blend may also reflect the effect of the defects on the HC phase structures.

4. Conclusion

In summary, the PEO crystal orientations within the 2D confined HC phase structure are studied by using the 2D SAXS and WAXD measurements. The samples used to generate the HC phase structures are either a diblock copolymer or a blend of the diblock copolymer with a PS homopolymer. Since, $T_{ODT} \gg T_g^{PS} > T_m^{PEO}$, the PEO block crystallization takes place in a 2D confined PS glassy environment. In these two samples, we have kept the two M_n^{PEO} to be almost identical. The confined space size (the diameter of the cylinders) and the tethering density of the PEO blocks at the interfaces are thus almost the same for these two samples. The c-axes orientation of the PEO crystals within the cylinders have been found to change from random, to tilt, and to perpendicular with respect to $\hat{a}$ as the T_c

increases. The relationships of the tilt angle's dependence on the T_c for both samples are superposed onto each other, indicating that the c-axis orientation in the PEO block crystals are not sensitive to the defects under the conditions of identical confined size and the tethering density of the PEO blocks at the interfaces. The difference of the crystallization behaviors between the copolymer and the blend is, however, significant. The PEO block crystallization seems to be defect-controlled, and the crystallinity of PEO blocks in the copolymer is much lower than that in the blend samples under our experimental conditions. The mean crystallite sizes of $D_{120,s}$ and $D_{120,l}$ and their T_c dependences, estimated using the Scherrer equation for both of the samples, are similar on the same length scale. However, one problem still remains, since both the confined size and the tethering density of the PEO blocks at the interfaces will affect the PEO crystal orientation; can we separate these two factors and study these two effects independently? One way to investigate this problem may be to use a triblock copolymer, which has semicrystalline polymer as the end blocks, such as PEO-b-PS-b-PEO, to build an HC nano-confinement (keeping the d to be identical). For this triblock copolymer, the tethering density will be double, and the confined size will be almost identical if the M_n^{PEO} of each block in the triblock copolymer is half of the M_n^{PEO} in the diblock copolymer. Investigations of crystal orientation changes and crystallization will enlighten our understanding of the effect of the tethering density on these crystalline behaviors.

Acknowledgements

References

[1] Hirata E, Ijitsu T, Hashimoto T, Kawai H. Polymer 1975;16:249.
[2] Viras F, Luo YZ, Viras K, Mobbs RH, King TA, Booth C. Makromol Chem 1988;189:459.
[3] Séguéla R, Prud'homme J. Polymer 1989;30:1446.
[4] Douzinas KC, Cohen RE. Macromolecules 1992;25:5030.
[5] Cohen RE, Bellare A, Drzewinski MA. Macromolecules 1994;27:2321.
[6] Yang YW, Tanodekaew S, Mai SM, Booth C, Ryan AJ, Bras W, et al. Macromolecules 1995;28:6029.
[7] Hamley IW, Fairclough JPA, Ryan AJ, Bates FS, Towns-Andrews E. Polymer 1996;37:4425.
[8] Hamley IW, Fairclough JPA, Terrill NJ, Ryan AJ, Lipic PM, Bates FS, et al. Macromolecules 1996;29:8835.
[9] Hillmyer MA, Bates FS. Macromol Symp 1997;117:121.
[10] Hamley IW, Wallwork ML, Smith DA, Fairclough JPA, Ryan AJ, Mai SM, et al. Polymer 1998;39:3321.
[11] Bates FS, Fredrickson GH. Annu Rev Phys Chem 1990;41:525.
[12] Zhu L, Chen Y, Zhang A, Calhoun BH, Chun M, Quirk RP, et al. Phys Rev B 1999;60:10022.
[13] Cohen RE, Cheng PL, Douzinas KC, Kofinas P, Berney CV. Macromolecules 1990;23:324.

[14] Sakurai K, MacKnight WJ, Lohse DJ, Schulz DN, Sissano JA. Macromolecules 1993;26:3236.

[15] Khandpur AK, Macosko CW, Bates FS. J Polym Sci, Part B: Polym Phys 1995;33:247.

[16] Zhao J, Majumdar B, Schulz MF, Bates FS, Almdal K, Mortensen K. Macromolecules 1996;29:1204.

[17] Weimann PA, Hajduk DA, Chu C, Chaffin KA, Brodil JC, Bates FS. J Polym Sci, Part B: Polym Phys 1999;37:2053.

[18] Zhu L, Cheng SZD, Calhoun BH, Ge Q, Quirk RP, Thomas EL, et al. J Am Chem Soc 2000;122:5957.

[19] Loo YL, Register RA, Ryan AJ, Dee GT. Macromolecules 2001;34:8968.

[20] Loo YL, Register RA, Ryan AJ. Macromolecules 2002;35:2365.

[21] Huang P, Zhu L, Cheng SZD, Ge Q, Quirk RP, Thomas EL, et al. Macromolecules 2001;34:6649.

[22] Quiram DJ, Register RA, Marchand GR. Macromolecules 1997;30:4551.

[23] Quiram DJ, Register RA, Marchand GR, Adamson DH. Macromolecules 1998;31:4891.

[24] Zhu L, Mimnaugh BR, Ge Q, Quirk RP, Cheng SZD, Thomas EL. Polymer 2001;42:9121.

[25] Huang P, Zhu L, Guo Y, Ge Q, Jing AJ, Chen WY, et al. Macromolecules 2004;37:3689.

[26] Zhu L, Cheng SZD, Calhoun BH, Ge Q, Quirk RP, Thomas EL, et al. Polymer 2001;42:5829.

[27] Quirk RP, Kim J, Kausch C, Chun MS. Polym Int 1996;39:3.

[28] Alexander LE. X-ray diffraction methods in polymer science. New York: Wiley–Interscience; 1969.

[29] Cheng SZD, Wunderlich B. J Polym Sci, Part B: Polym Phys 1986;24: 577.

[30] Trent JS, Scheinbeim JI, Couchman PR. Macromolecules 1983;16:589.

[31] Chen WY, Zheng JX, Cheng SZD, Li CY, Huang P, Zhu L, et al. Phys Rev Lett 2004;93:028301.

[32] Takahashi Y, Tadokoro H. Macromolecules 1973;6:672.

[33] Zhu L, Calhoun BH, Ge Q, Quirk RP, Cheng SZD, Thomas EL, et al. Macromolecules 2001;34:1244.

[34] Müller AJ, Balsamo V, Arnal ML, Jakob T, Schmalz H, Abetz V. Macromolecules 2002;35:3048.

[35] Reiter G, Castelein G, Sommer JU, Röttele A, Thurn-Albrecht T. Phys Rev Lett 2001;87:226101.

[36] Lee W, Chen H, Lin T. J Polym Sci, Part B: Polym Phys 2002;40:519.

[37] Xu JT, Turner SC, Fairclough JPA, Mai SM, Ryan AJ, Chaibundit C, et al. Macromolecules 2002;35:3614.

[38] Xu JT, Fairclough JPA, Mai SM, Ryan AJ, Chaibundit C. Macromolecules 2002;35:6937.

[39] Schmalz H, Müller AJ, Abetz V. Macromol Chem Phys 2003;204:111.

[40] Sun L, Zhu L, Ge Q, Quirk RP, Xue C, Cheng SZD, et al. Polymer 2004; 45:2931.

[41] Arnal ML, López-Carrasquero F, Laredo E, Müller AJ. Euro Polym J 2004;40:1461.